Check for updates

ORIGINAL RESEARCH

Rhinovirus C15 Induces Airway Hyperresponsiveness via Calcium Mobilization in Airway Smooth Muscle

Vishal Parikh[1], Jacqueline Scala[1], Riva Patel[1], Corinne Corbi[1], Dennis Lo[1], Yury A. Bochkov[2], Joshua L. Kennedy[3], Richard C. Kurten[4], Stephen B. Liggett[5,6], James E. Gern[2], and Cynthia J. Koziol-White[1]

[1]Robert Wood Johnson Medical School, Rutgers University, New Brunswick, New Jersey; [2]Department of Pediatrics, University of Wisconsin–Madison, Madison, Wisconsin; [3]Department of Pediatrics and [4]Department of Physiology and Biophysics, University of Arkansas for Medical Sciences, Little Rock, Arkansas; and [5]Department of Molecular Pharmacology and Physiology and [6]Department of Medicine, University of South Florida Morsani College of Medicine, Tampa, Florida

Abstract

Rhinovirus (RV) exposure evokes exacerbations of asthma that markedly impact morbidity and mortality worldwide. The mechanisms by which RV induces airway hyperresponsiveness (AHR) or by which specific RV serotypes differentially evoke AHR remain unknown. We posit that RV infection evokes AHR and inflammatory mediator release, which correlate with degrees of RV infection. Furthermore, we posit that rhinovirus C–induced AHR requires paracrine or autocrine mediator release from epithelium that modulates agonist-induced calcium mobilization in human airway smooth muscle. In these studies, we used an *ex vivo* model to measure bronchoconstriction and mediator release from infected airways in human precision cut lung slices to understand how RV exposure alters airway constriction. We found that rhinovirus C15 (RV-C15) infection augmented carbachol-induced airway narrowing and significantly increased release of IP-10 (IFN-γ–induced protein 10) and MIP-1β (macrophage inflammatory protein-1β) but not IL-6. RV-C15 infection of human airway epithelial cells augmented agonist-induced intracellular calcium flux and phosphorylation of myosin light chain in co-cultured human airway smooth muscle to carbachol, but not after histamine stimulation. Our data suggest that RV-C15–induced structural cell inflammatory responses are associated with viral load but that inflammatory responses and alterations in agonist-mediated constriction of human small airways are uncoupled from viral load of the tissue.

Keywords: asthma; rhinovirus; bronchitis; wheezing; exacerbations

Rhinovirus (RV) exposure frequently evokes asthma exacerbations in adult and pediatric populations. Although it is well understood that airway hyperresponsiveness (AHR) is a key contributor to asthma exacerbations, the underlying mechanisms by which RV infection evokes AHR are undefined. Several model systems have been used to study the effects of RVs, including single-cell–type culture systems, co-culture systems of different cell types, murine model systems, and *in vivo* human studies of RV exposure (1–12).

RVs are single-stranded, positive sense RNA enteroviruses that for many years were classified on the basis of immunoreactivity to antibodies, and individual RVs were termed "serotypes." Using whole-genome sequencing, we have now shown that RVs consist of over 160 genetically defined types

(Received in original form January 2, 2019; accepted in final form September 18, 2019)

Supported by National Institutes of Health (NIH) grants P01-HL114471-03 (S.B.L. and C.J.K.-W.); NIH UL1TR003017 (C.J.K.-W.); 1K08A1121345-01A1, KL2TR000063, UL1TR000039, P20GM121293, and P20GM103625 (J.L.K.); and U19 AI104317 and P01 HL070831 (Y.A.B. and J.E.G.).

Author Contributions: V.P.: study design, data acquisition, data analysis and interpretation, drafting and editing of the manuscript, and final approval of publication. J.S.: study design, data acquisition, data analysis and interpretation, editing of the manuscript, and final approval of publication. R.P.: data acquisition, data analysis and interpretation, drafting and editing of the manuscript, and final approval of publication. C.C.: data acquisition, data analysis and interpretation, drafting and editing of the manuscript, and final approval of publication. D.L.: data acquisition, data analysis and interpretation, drafting and editing of the manuscript, and final approval of publication. Y.A.B.: study design, data interpretation, drafting and editing of the manuscript, and final approval of publication. J.L.K.: study design, drafting and editing of the manuscript, and final approval of publication. R.C.K.: study design, drafting and editing of the manuscript, and final approval of publication. S.B.L.: study design, drafting and editing of the manuscript, and final approval of publication. J.E.G.: study design, drafting and editing of the manuscript, and final approval of publication. C.J.K.-W.: study design, data acquisition, data analysis and interpretation, drafting and editing of the manuscript, and final approval of publication.

Correspondence and requests for reprints should be addressed Cynthia J. Koziol-White, Ph.D., Rutgers Institute for Translational Medicine and Science, Child Health Institute of New Jersey, 89 French Street, Room 4268, New Brunswick, NJ 08901. E-mail: cjk167@rbhs.rutgers.edu.

This article has a data supplement, which is accessible from this issue's table of contents at www.atsjournals.org.

Am J Respir Cell Mol Biol Vol 62, Iss 3, pp 310–318, Mar 2020
Copyright © 2020 by the American Thoracic Society
Originally Published in Press as DOI: 10.1165/rcmb.2019-0004OC on September 18, 2019
Internet address: www.atsjournals.org

within three species: RV-A, RV-B, and RV-C (13). These findings arose from studies in which sequencing approaches ascertained the complete genomes of all named RV serotypes, as well as field isolates, with subsequent phylogenetic relationships determined. Various studies suggest heterogeneity of the inflammatory or AHR phenotypes among different RVs (1, 3, 12, 14–23).

Recently, RV-C was identified in multiple field studies of wheezing children (13, 24, 25) and may be associated with severe disease (26, 27). Although RV-C strains are difficult to propagate in culture (2, 28–30), we have successfully grown and sequenced a representative strain termed "rhinovirus C15" (RV-C15) (24, 25, 30). Studies have shown that some RV species are most prevalent in children and adults during wheezing illnesses. For example, Xiao and colleagues demonstrated that RV-C, rather than RV-A or RV-B serotype, was most commonly present in nasopharyngeal aspirates of wheezing children (31). Given these data, we chose to study RV-C15 on the basis of associations with asthma exacerbations and human airway disease. We used human precision cut lung slices (hPCLS) to study the physiologic and biochemical responses after RV infection, and we cultured primary human airway epithelial cells (HAEC) and human airway smooth muscle cells (HASM) from the same donor to assess changes in agonist-induced contractile signaling after RV infection of the epithelium.

Methods

Materials

Carbachol (carbamoyl choline chloride [Cch]), histamine (histamine dihydrochloride [Hist]), and perchloric acid were purchased from Sigma-Aldrich. Antibodies for detection of phosphorylated Akt, pMLC (phosphorylated myosin light chain), and Akt were purchased from Cell Signaling Technology. Myosin light chain (MLC) antibody was purchased from EMD Millipore. Radioimmunoprecipitation assay buffer was purchased from Cell Signaling Technology. RV-C15 was produced by RNA transfection; clarified lysates were treated with RNase A; and virus was purified by ultracentrifugation through a 30% sucrose cushion.

hPCLS Preparation and Measurement of Bronchoconstriction

hPCLS were prepared as previously described (32). Human lung tissue from aborted lung transplants was obtained from anonymous donors according to procedures approved by the Rutgers University Institutional Review Board. The hPCLS were derived from nonasthma lung donors with no history of chronic disease or smoking, with donor demographics shown in Table E1 in the data supplement. Briefly, whole human lungs were dissected and inflated using 2% (wt/vol) low–melting-point agarose. Once the agarose was set, the lung lobes were sectioned, and cores of 8 mm diameter were made. The cores that contained a small airway by visual inspection were sliced at a thickness of 350 μm (VF300 Vibratome; Precisionary Instruments) and collected in wells containing supplemented Ham's F-12 medium. Suitable airways (≤1-mm diameter) in slices were selected on the basis of the following criteria: presence of a full smooth muscle wall, presence of beating cilia, and unshared muscle walls at airway branch points to eliminate possible counteracting contractile forces. Slices were incubated at 37°C in a humidified air/CO_2 (95%/5%) incubator and were rinsed with fresh media two or three times to remove agarose and endogenous substances released that variably confound the production of inflammatory mediators and/or alter airway tone. Slices were then incubated with diluent (dilution of 30% sucrose solution) or RV-C15 (10^5–10^7 plaque-forming unit (pfu), produced by reverse genetics [30]). hPCLS were exposed to RV (or diluent) at the indicated concentrations for 48 hours before the bronchoconstrictive response to Cch was tested. Slices were washed with media and then exposed to a dose response (10^{-8}–10^{-4} M) of Cch, and the luminal area was measured to calculate bronchoconstriction compared with baseline.

Luminal area measurements were performed using methods previously described in detail (32). Briefly, lung slices were placed in a 12-well plate in media and held in place using a nylon weight with platinum attachments. The airway was located using a microscope (magnification, ×40; Nikon Eclipse, model no. TE2000-U; Nikon Instruments) connected to a live video feed (Evolution QEi, model no. 32-0074A-130 video recorder; MediaCybernetics). Airway luminal area was measured using Image-Pro Plus software (version 6.0; MediaCybernetics) and represented in units of square micrometers (33). The luminal area of each airway at baseline and at each Cch dose was calculated using Image-Pro Plus software, and percentage bronchoconstriction was plotted against increasing Cch concentrations and fit to a sigmoidal dose–response curve. Maximal bronchoconstriction, a measure of the sensitivity of the airways to Cch (log of the effective concentration to induce 50% bronchoconstriction [Log EC_{50}]), and the integrated response to contractile agonist, defined as the area under the curve (AUC), were calculated from the dose–response curves generated using Prism software (version 5; GraphPad Software) and compared.

Isolation and Cultivation of HASM and HAEC

HASM cells were derived from tracheas obtained from the National Disease Research Interchange and from the International Institute for the Advancement of Medicine. HASM cell culture was performed as described previously (34). The cells were cultured in Ham's F-12 medium supplemented with 10% FBS, 100 U/ml penicillin, 0.1 mg/ml streptomycin, and 2.5 mg/ml amphotericin B, and this medium was replaced every 72 hours. HASM cells in subculture during passages 1–5 were used, because these cells retain the expression of native contractile protein, as demonstrated by immunocytochemical staining for ACTA2 and myosin (34). HAEC were derived from the same tracheas from which the HASM were derived. The cells were cultured on Transwell inserts (Corning) and fed both apically and basally with Pneumacult-Ex Basal Media (STEMCELL Technologies) until confluent. The cells were then differentiated at the air–liquid interface (ALI) for 21 days before stimulation. The HASM and HAEC were derived from nonasthma donors, as shown in Table E1.

Inflammatory Mediator Analysis

Tissue culture supernatants were obtained from the same slices that were used for the

contractility experiments. Inflammatory mediator analysis was performed using single-analyte ELISAs (R&D Systems) for IL-6, MIP-1β (macrophage inflammatory protein-1β), and IP-10 (IFN-γ–induced protein 10) ($n = 6$ donors with ⩾3 slices/condition). Data are expressed as picograms of mediator concentrations divided by total protein content of tissue culture supernatants, and as fold change of RV stimulated compared with diluent stimulated.

Detection of RV RNA

Slices were washed after the incubation with RV and processed for mRNA extraction. Briefly, hPCLS were pooled for each treatment, suspended in RNA lysis buffer, and lysed using a TissueLyser (Qiagen). Lysates were then run through a QIAshredder column before purification using the RNeasy kit (Qiagen). The mRNA isolated was converted to cDNA using the ThermoScript RT-PCR kit (Thermo Fisher Scientific). Viral load from the cDNA generated was assessed by qPCR using Power SYBR Green PCR Master Mix (Applied Biosystems) with the following primers: forward primer: 5′-CCTCCGGCCCCTGAAT-3′; reverse primer: 5′-AAACACGGACACCC AAAGTAGT-3′. Viral load was expressed both as raw numbers (pfu of replicates run) and as fold change of RV stimulated compared with diluent stimulated, because some tissue may already have been exposed to other types of RV. (Baseline concentrations of RV were detected in some samples.)

Immunoblot Analysis

Confluent ALI-differentiated HAEC plated on Transwell inserts were exposed to RV-C15 (10^6 pfu = multiplicity of infection ~1; 48 h) with HASM medium cultured under the insert. HAEC-conditioned medium was transferred to serum-starved HASM cells for 48 hours. Cells were then stimulated with Cch (10 μM; 10 min) or Hist (1 μM; 10 min). Cells were then treated with 500 μM perchloric acid; plates were scraped; and cells were pelleted. Pellets were solubilized in radioimmunoprecipitation assay buffer before being subjected to SDS-PAGE and transferred to nitrocellulose membranes, as previously described (35). pMLC (Cell Signaling Technology) and pAkt (Cell Signaling Technology) were assessed, and band densities were normalized to total MLC (anti-MLC-2; EMD Millipore) and Akt (Cell Signaling Technology).

Intracellular Calcium Flux Measurement

$[Ca^{2+}]_i$ was measured using the Fluo-8 Calcium Flux Assay Kit (Abcam). Confluent HASM cells were incubated with Fluo-8 dye for 1 hour at 37°C. After Fluo-8 incubation, fluorescence intensity was measured using the CLARIOstar microplate reader (BMG LABTECH). Baseline fluorescence intensity was measured for 10 seconds; Cch (10 μM final; Sigma-Aldrich) was autoinjected into the well; and fluorescence intensity was measured for 160 seconds. $[Ca^{2+}]_i$ fluorescence intensity was normalized to baseline fluorescence intensity.

Statistical Analysis

GraphPad Prism software was used to determine normality of the distribution of the data (raw values as well as fold change compared with control buffer) and statistical significance. Normality was assessed via D'Agostino and Pearson omnibus normality test before either *t* test or ANOVA. Statistical significance (both compared with buffer control, as well as between the conditions for a given experiment) was evaluated via unpaired Student's *t* tests for two-group comparisons or ANOVA for multiple-group comparisons with either Bonferroni's or Dunn's posttest, depending on the normality of the distribution of the data for the hPCLS data. For the HASM data, paired Student's *t* tests for two-group comparisons were used to assess significance. *P* values less than 0.05 were considered significant. Associations between parameters were assessed using linear regression analysis, with R^2 and *P* values reported in the text and Table 1.

Results

RV-C15 Infection Increased Sensitivity to Cch-induced Bronchoconstriction

hPCLS were prepared from nonasthma lung donors and infected with RV-C15 (10^5–10^7 pfu) for 48 hours. Bronchoconstriction in response to Cch, a muscarinic receptor agonist, was assessed in slices and compared with that treated with diluent. With diluent alone (no virus; control), the EC_{50} for Cch-mediated constriction was approximately 3 μM. As shown in Figure 1, RV-C15 exposure induced a 100-fold leftward shift in the cumulative response curve for Cch with an EC_{50} of approximately 0.03 μM. In addition, the AUC at this concentration of virus increased by approximately 40% compared with diluent. The maximal constriction was unaffected. Interestingly, although studies show that RV-A and RV-C serotypes are associated with more severe asthma exacerbations, many RV-A strains had little effect on airway responsiveness to Cch

Table 1. Linear Regression Analysis Comparing Contractile and Inflammatory Parameters with Viral Load

Variables Plotted (Fold Change vs. Control)	R^2 Value	*P* Value
IP-10 release vs. RV-C15 detected	0.28	0.36
IL-6 release vs. RV-C15 detected	0.22	0.42
MIP-1β vs. RV-C15 detected	0.96	0.003
Change in sensitivity (Log EC_{50}) vs. RV-C15 detected	0.29	0.35
Change in total response (AUC) vs. RV-C15	0.03	0.79
IP-10 release vs. change in total response (AUC)	0.14	0.53
IL-6 release vs. change in total response (AUC)	0.86	0.02
MIP-1β vs. change in total response (AUC)	0.05	0.71
Change in sensitivity (Log EC_{50}) vs. IL-6 release	0.01	0.87
Change in sensitivity (Log EC_{50}) vs. IP-10 release	0.06	0.69
Change in sensitivity (Log EC_{50}) vs. MIP-1β release	0.45	0.45

Definition of abbreviations: AUC = area under the curve; IP-10 = IFN-γ–induced protein 10; Log EC_{50} = log of effective concentration to induce 50% bronchoconstriction; MIP-1β = macrophage inflammatory protein-1β; RV-C15 = rhinovirus C15.
Data represent $n = 5$ separate donors.

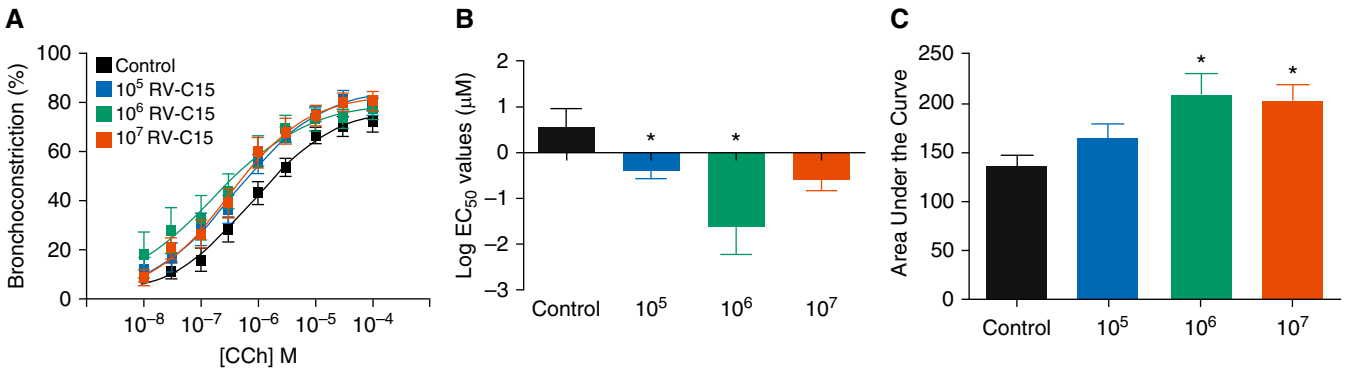

Figure 1. Rhinovirus C15 (RV-C15) significantly increases airway reactivity to carbachol (Cch)-induced bronchoconstriction. Human precision cut lung slices were stimulated with RV-C15 (10^5–10^7 pfu) or diluent for 48 hours. Constriction of small airways within each slice was assessed to a Cch dose response (10^{-8}–10^{-4} M). (*A–C*) Dose–response curves (*A*), log of the effective concentration to induce 50% bronchoconstriction (Log EC_{50}) values (*B*), and area under the curve (*C*) were plotted and compared. Data represent $n = 5$ separate donors with at least three slices/treatment for each donor (mean ± SEM). *$P < 0.05$. Two-tailed unpaired *t* tests comparing each condition with control buffer, as well as a two-way ANOVA, were performed. pfu = plaque-forming unit.

(Figure E1). These data are consistent with our previous observations (5). Taken together, these results suggest that RV-C15 enhanced Cch-mediated airway constriction by increasing the sensitivity of the airways to a contractile agonist, as well as by increasing the overall response, represented by the AUC.

RV-C15 Infects hPCLS and Elicits Mediator Release, whereas Viral Load Correlates with Levels of MIP-1β, IL-6, and Cch-induced Bronchoconstriction

RV-C15 RNA was detected at concentrations significantly above control buffer–stimulated tissue, but the fold increase between doses of RV-C15 was similar over the dose response (Figure 2). We found that RV-C15 increased supernatant concentrations of IP-10, IL-6, and MIP-1β, but there was little difference in release among doses of RV-C15 (Figure 3). Interestingly, exposure to RV-C15 had little effect on concentrations of TNF-α, IL-1β, IL-33, TGF-β (transforming growth factor-β), or IL-13 (Table E2), cytokines or growth factors known to induce AHR in hPCLS or augment agonist-induced contractile signaling in HASM (32, 33, 36–40). After exposure to RV-C15, a correlation was found between viral load (at 10^7 pfu treatment condition/control buffer) and MIP-1β release ($R^2 = 0.96$; $P = 0.003$) (Table 1). To determine if there were any associations between RV-C15–induced AHR, mediator release, and viral load, we used linear regression analysis of the following parameters: changes in sensitivity of the airways to Cch; the magnitude of the response (AUC); viral load; and release of IP-10, IL-6, or MIP-1β. IP-10, IL-6, or MIP-1β concentrations served as surrogates of RV-induced inflammatory markers. Our data show that increased MIP-1β or IP-10 concentrations were poorly correlated with changes in sensitivity of the airways or total response, but that IL-6 correlated with change in total response to Cch-induced bronchoconstriction ($R^2 = 0.86$; $P = 0.02$) (Table 1).

RV-C15 Infection Enhances Agonist-induced Intracellular Calcium Flux and pMLC but Not pAkt

To address the molecular mechanisms by which RV-C15 promotes AHR, we used a media transfer model of an RV-C15–infected, ALI-differentiated HAEC to HASM. To date, few studies have used a co-culture model of HAEC with HASM to interrogate interactions between these cell types after RV-A16 exposure (10, 41). Given the hyperresponsiveness observed after RV-C15 exposure of hPCLS, we hypothesized that exposure of HAEC to RV-C15 would enhance agonist-induced contractile pathways in HASM to induce AHR. We stimulated HAEC (10^6 pfu; 48 h) and measured agonist-induced calcium flux and pMLC and Akt (pAkt) in HASM after media transfer from the HAEC to the HASM. We demonstrate that after HAEC exposure to RV-C15, Cch- but not Hist-induced intracellular calcium flux in HASM was augmented compared with buffer control stimulation of HAEC (Figure 4). Cch and Hist alone induced pMLC, but only Cch- and not Hist-induced pMLC in HASM was augmented after HAEC exposure to RV-C15 (Figure 5). We previously demonstrated that Cch-induced activation of PI3K p110δ induced and maintained pMLC. To ascertain whether RV-C15 exposure was inducing augmented pMLC through this pathway, we examined agonist-induced Akt phosphorylation (pAkt, a surrogate readout of PI3K activation) in HASM in the absence and presence of RV-C15 exposure of HAEC. We show that Cch, but not Hist, induces pAkt. Unlike pMLC,

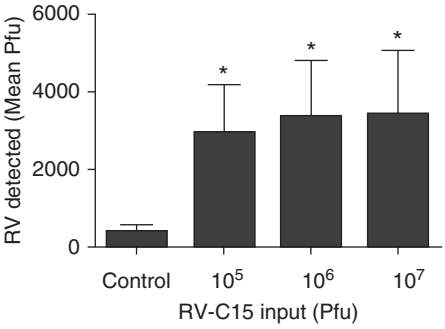

Figure 2. Viral load significantly increased after exposure to RV-C15. Data represent means for $n = 6$ separate donors for RV-C15. *$P < 0.05$ compared with control buffer. There was no significant increase in virus detection between amounts of RV input. Two-tailed paired *t* tests comparing each condition with control buffer were performed, as was two-way ANOVA.

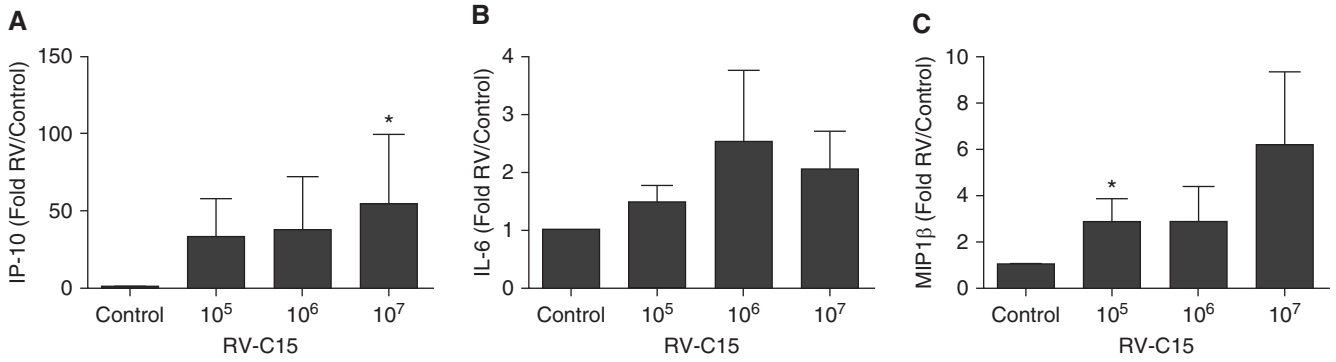

Figure 3. RV-C15 induces release of (*A*) IP-10 (IFN-γ–induced protein 10), (*B*) IL-6, and (*C*) MIP-1β (macrophage inflammatory protein-1β), but concentrations are not significantly different between input doses of virus. Data represent $n = 5$ separate donors with at least three slices/treatment for each donor (mean ± SEM). Data are expressed as fold change compared with control. Two-tailed paired *t* tests comparing each condition with control buffer were performed, as was two-way ANOVA. $^*P < 0.05$ compared with control.

Cch-induced pAkt phosphorylation is not augmented by exposure to RV-C15 (Figure 6). Given that RV-A and RV-C serotypes have been postulated to induce severe asthma exacerbations, we next examined whether RV-A16 exposure of HAEC altered agonist-induced calcium concentrations in HASM. We demonstrate that unlike exposure to RV-C15, HAEC exposure to RV-A16 had little effect on Cch-induced calcium mobilization in HASM (Figure E2). Taken together, our findings suggest that RV-C15 exposure of HAEC modulates muscarinic receptor–induced contractile signaling in HASM through calcium mobilization pathways to enhance potential contraction through actin–myosin cross-bridging.

Discussion

RV infection represents the leading cause of exacerbations of underlying airway diseases and has been postulated to be important in the development of asthma. *In vitro* studies have mainly focused on RV-A and RV-B serotype exposure of single cells, with few using an integrated cell- or tissue-based

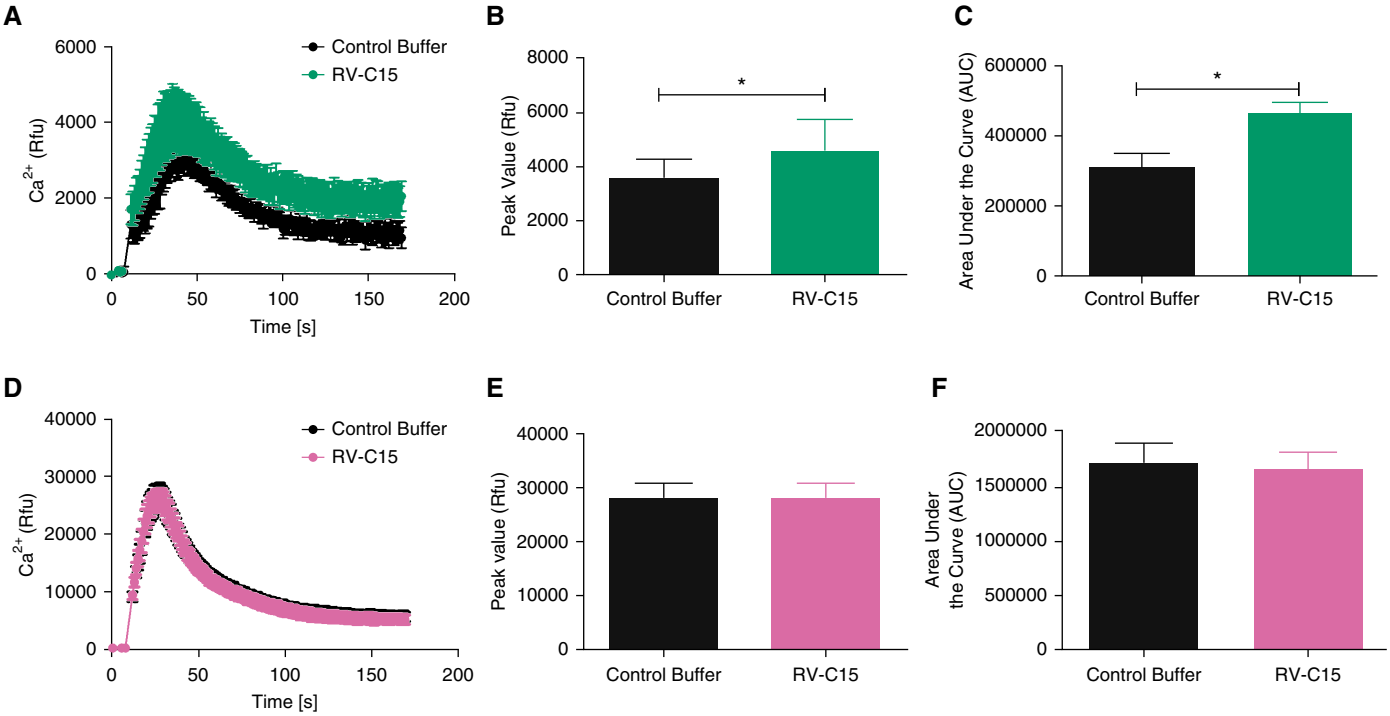

Figure 4. RV-C15 augments Cch- but not histamine (Hist)-induced intracellular calcium flux. Human airway epithelial cells (HAEC) were exposed to RV-C15 (10^6 pfu; 48 h). (*A–F*) Conditioned medium was transferred to serum-starved human airway smooth muscle (HASM), and intracellular calcium flux (Fluo-8 dye) was measured after (*A–C*; green) Cch (10 μM) or (*D–F*; purple) Hist (1 μM) stimulation. (*A–F*) Time courses after agonist stimulation (*A* and *D*), peak calcium response (*B* and *E*), and area under the curve (*C* and *F*) are shown. Data represent mean ± SEM of four separate donors. $^*P < 0.05$ compared with control buffer. Two-tailed paired *t* tests comparing each condition with control buffer were performed, as was two-way ANOVA. Rfu = relative fluorescence units.

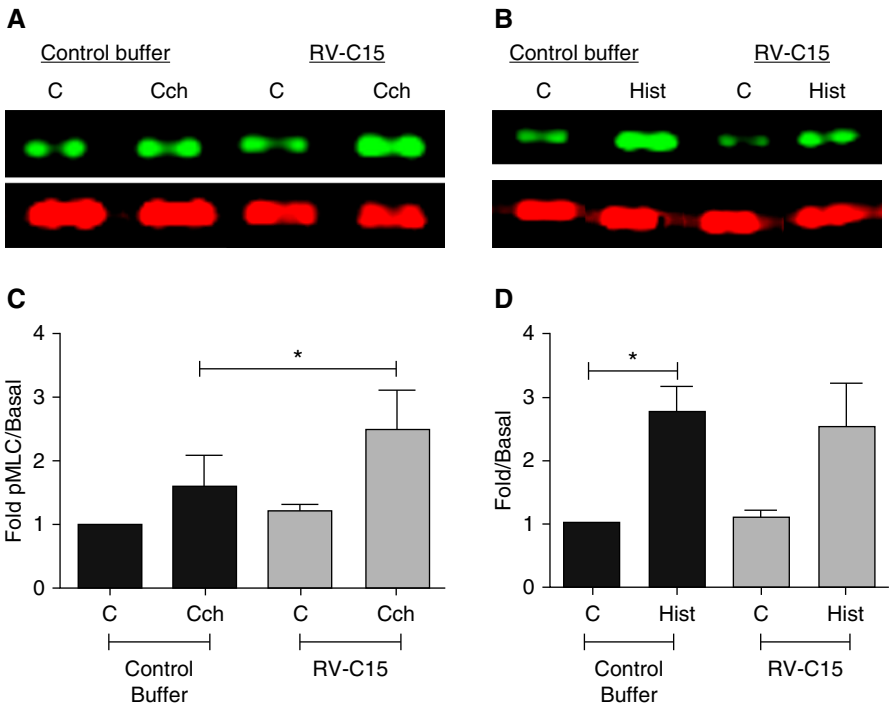

Figure 5. RV-C15 augments Cch- but not Hist-induced phosphorylated myosin light chain (pMLC). HAEC were exposed to RV-C15 (10^6 pfu; 48 h) or control buffer. (*A–D*) Conditioned medium was transferred to serum-starved HASM, and cells were stimulated with Cch (10 μM; 10 min) (*A* and *C*) or Hist (1 μM; 10 min) (*B* and *D*). pMLC was assessed, normalized to total myosin light chain, and expressed as fold change compared with unstimulated control. Data represent mean ± SEM of three separate donors. Lanes shown in *B* are from the same gel (*see* Figure E4 for full-length gel). $^*P < 0.05$. Two-tailed paired *t* tests comparing each condition with its respective control buffer were performed. C = control.

platform. A number of groups have examined whether the RV-A or RV-C serotype elicits greater inflammation and symptoms. Nakagome and colleagues demonstrated that exposure of ALI-differentiated epithelial cells to RV-A, RV-B, and RV-C serotypes elicited inflammatory mediator release that was equivalent among RV-A and RV-C serotypes, but RV-B serotypes elicited diminished concentrations, which was attributed to slower rates of replication of RV-B serotypes (8). In children and adults, RV-A and RV-C serotypes were commonly identified in clinical samples from subjects, and wheezing in subjects was more often associated with the presence of RV-A and RV-C rather than RV-B (42). Our studies used hPCLS and HAEC/HASM co-cultures derived from non-diseased donors to examine the effects of RV-C15 exposure on structural cells of the airways, inflammatory mediator concentrations, and alterations in contractility of the airways. We used small airways and structural cells isolated from human lungs infected with RV-C15 for 48 hours to examine all of our parameters, physiologic and inflammatory, on the basis of two lines of evidence: *1*) clinical observations by other investigators after RV exposure and *2*) our own studies showing that amplification of contractile agonist–induced bronchoconstriction and mediator concentrations are augmented consistent with a late-phase response to virus (data not shown). We found that RV-C15 augmented Cch-induced bronchoconstriction in hPCLS (Figure 1). Although numerous studies demonstrate that RV-A and RV-C serotypes are associated with severe asthma exacerbations, we did not observe increased airway responsiveness to many RV-A strains (Figure E1), which is consistent with our previous observations (5).

The idea that increased viral load equates to greater symptom burden has been fairly widely accepted until relatively recently. Kennedy and colleagues demonstrated in a cohort exposed to RV-A16 that there were no differences in viral load in children and adults with and without asthma and that atopic status had no bearing on viral load detected (6). Another study suggested that viral infection is critical to the enhancement of mediator release and airway inflammation (43). A study of a pediatric population with asthma found that RV was associated with asthma exacerbations, but that type III IFN-λ1 concentrations measured were a strong predictor of wheezing, regardless of the presence of RV in the samples. Interestingly, of the children with detectable RV, the viral load measured was not different between those who were wheezing and those who were not (44). These investigators showed little association among inflammatory mediators released after RV exposure and wheezing. In pediatric and adult subjects after RV infection, greater than 10^5 RNA copies per milliliter (considered to be high amounts of virus detected) manifested upper and lower respiratory symptoms, but the viral load was poorly correlated with the kinetics of the clinical symptoms (45). In our *ex vivo* hPCLS system, we found that RV-C15 viral load correlated with RV-C15–induced concentrations of MIP-1β and in part concentrations of IL-6. However, we showed no association between viral load and increased AHR after RV-C15 infection. Our data suggest that viral load is uncoupled from AHR and that our measured inflammatory responses to virus are not associated with AHR. Viral load, however, correlated with increased concentrations of MIP-1β and IL-6. Further studies are needed to characterize whether donor and underlying disease states modulate viral responses and AHR.

Studies in our laboratory and others have noted that inflammatory mediators enhance responses to contractile agonists. Therefore, we hypothesized that after RV-C15 exposure of HAEC, HASM exposed to HAEC-conditioned media would show augmented contractile signaling. The enhancement of contractile signaling we observed in the hPCLS would therefore be mimicked in an *in vitro* cell system. To test this, we examined intracellular calcium flux,

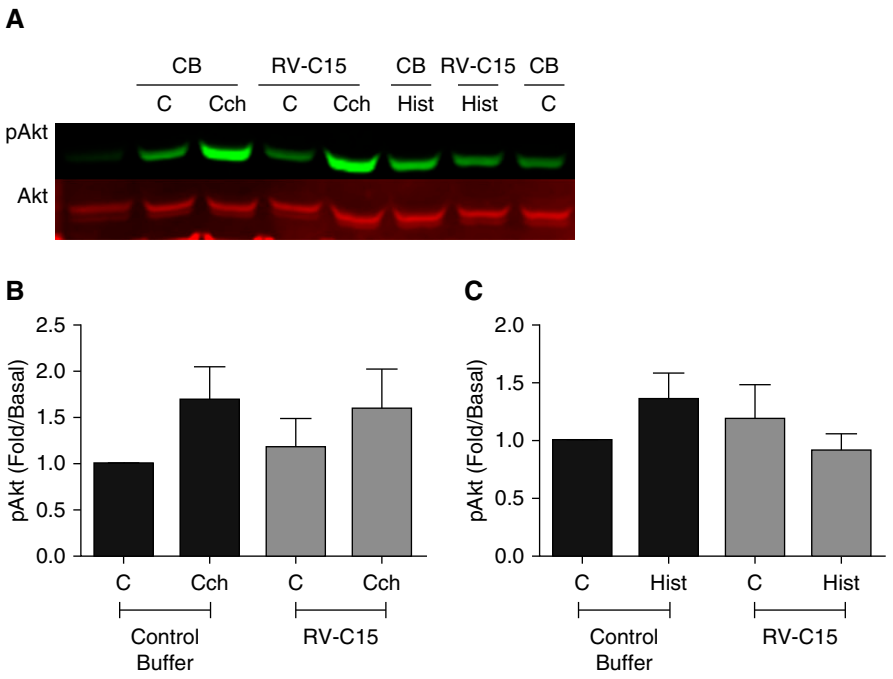

Figure 6. RV-C15 does not augment Cch- or Hist-induced phosphorylation of Akt (pAkt). HAEC were exposed to RV-C15 (10^6 pfu; 48 h) or control buffer (CB). Conditioned medium was transferred to serum-starved HASM, and cells were stimulated with (*A* and *B*) Cch (10 μM; 10 min) or (*A* and *C*) Hist (1 μM; 10 min). pAkt was assessed and normalized to total Akt. Data represent mean ± SEM of three separate donors. *P* = not significant. Two-tailed paired *t* tests comparing each condition with control buffer were performed, as was two-way ANOVA.

pMLC, and activation of PI3K (pAkt), markers of contractile signaling in HASM, some of which are augmented after exposure to inflammatory mediators (32, 39). We demonstrate that Cch-induced intracellular calcium flux and pMLC, but not pAkt, are augmented after RV-C15 exposure. Stimulation with Hist demonstrated that the augmentation of agonist-mediated calcium flux and pMLC is agonist selective after RV-C15 exposure. These data suggest that RV-C15–dependent augmentation of Cch-induced HASM contraction occurs through calcium-dependent mechanisms. In other cell types, changes in intracellular calcium flux mediate processes such as viral entry into the cell, activation of cell stress and apoptosis, propagation of the virus, and modulation of an inflammatory response (46–48), with there being a direct interaction between RV and different cell types, including immunocytes and epithelial cells. Our system, however, shows that, in the absence of direct cell contact between RV-C15 and HASM, exposure of HAEC to RV-C15 elicits greater Cch-induced intracellular calcium flux in HASM, suggesting that release of a soluble mediator(s) from HAEC may modulate the augmented contractility of the HASM that we observed. Accordingly, we sought to identify whether mediators that we and others have shown to induce AHR in hPCLS or in HASM (32, 33, 36–40) were increased by RV-C15 exposure in hPCLS or HAEC. Exposure to RV-C15 had little effect on TNF-α, IL-1β, IL-33, TGF-β, or IL-13 release (Table E2). Because RV-A and RV-C serotypes have been postulated to precipitate severe asthma exacerbations, we next examined the effect of RV-A16 exposure of HAEC on agonist-induced calcium flux in HASM. We demonstrated that, unlike exposure to RV-C15, HAEC exposure to RV-A16 had little effect on Cch-induced intracellular calcium flux in HASM (Figure E2). Our studies also show that structural cells of the airways are the likely targets that respond to RV to evoke AHR, because our observations occur in the absence of inflammatory cells. To our knowledge, our study is the first to show that RV exposure of airway cells modulates contractility of the airways via augmentation of calcium-dependent signaling in HASM.

Although our system has the advantage of being intact lung tissue and a complex multicellular system, our model has limitations. hPCLS lacks circulating immune cells, and therefore our findings need to be interpreted within this context. However, the integrated hPCLS model contains cells, including epithelial cells and airway smooth muscle cells, providing intact cell layers that would be among the first cell types to be exposed to inhaled RV. In addition, the presence of small airways within each lung slice allows us to measure both inflammatory mediator release and contractile responses of the airways from structural cells in their native state in the lungs. Our studies were performed in lungs procured from subjects without asthma. Clinical studies have noted that exposure to a single RV-A strain elicited increased symptoms in subjects with asthma compared with subjects without asthma (6, 12, 43, 49, 50). Recently, we demonstrated that there was an increase in responsiveness to a single dose of Cch after exposure to RV-A39 in hPCLS derived from subjects with mild to moderate asthma. Similar to the clinical studies, we found that exposure to RV-A39 failed to elicit enhanced responsiveness of the airways to Cch (5). In contrast to RV-A39, our data show that RV-C15 exposure induces AHR in a non-diseased lung. We and others have demonstrated that HASM derived from subjects with asthma exhibits a hypercontractile phenotype (32, 51–56), so using lungs and tissue from subjects with asthma may make it difficult to ascertain the effects of RV-C exposure on airway contractility, owing to an already hypercontractile system. Concentrations of IL-6 correlated with increased responsiveness of the airways to contractile agonist (Table 1). However, we demonstrate that there is no significant induction of IL-6 in response to RV-C15 exposure. IL-6 is reportedly a nonselective stress/inflammatory signal that is elicited by a number of different factors. It is conceivable that RV-C15 is incapable of inducing IL-6 to concentrations greater than what is observed at baseline, because the process of tissue slicing induces injury that increases basal concentrations of IL-6 in hPCLS.

Our data demonstrate that an integrated model of human lung provides an effective platform to predict RV-A and RV-C serotype–mediated AHR and structural cell responses, even in the absence of circulating immune cells. Our findings also support the hypothesis that infection/viral load is uncoupled from inflammatory mediator release and the responsiveness of the airways to contractile agonist–induced bronchoconstriction. ■

Author disclosures are available with the text of this article at www.atsjournals.org.

Acknowledgment: The authors thank Gaoyuan Cao and Brian Deeney for expert technical assistance.

References

1. de Kluijver J, Grünberg K, Sont JK, Hoogeveen M, van Schadewijk WA, de Klerk EP, *et al*. Rhinovirus infection in nonasthmatic subjects: effects on intrapulmonary airways. *Eur Respir J* 2002;20:274–279.
2. Griggs TF, Bochkov YA, Basnet S, Pasic TR, Brockman-Schneider RA, Palmenberg AC, *et al*. Rhinovirus C targets ciliated airway epithelial cells. *Respir Res* 2017;18:84.
3. Grünberg K, Timmers MC, de Klerk EP, Dick EC, Sterk PJ. Experimental rhinovirus 16 infection causes variable airway obstruction in subjects with atopic asthma. *Am J Respir Crit Care Med* 1999;160:1375–1380.
4. Grünberg K, Timmers MC, Smits HH, de Klerk EP, Dick EC, Spaan WJ, *et al*. Effect of experimental rhinovirus 16 colds on airway hyperresponsiveness to histamine and interleukin-8 in nasal lavage in asthmatic subjects *in vivo*. *Clin Exp Allergy* 1997;27:36–45.
5. Kennedy JL, Koziol-White CJ, Jeffus S, Rettiganti MR, Fisher P, Kurten M, *et al*. Effects of rhinovirus 39 infection on airway hyperresponsiveness to carbachol in human airways precision cut lung slices. *J Allergy Clin Immunol* 2018;141:1887–1890, e1.
6. Kennedy JL, Shaker M, McMeen V, Gern J, Carper H, Murphy D, *et al*. Comparison of viral load in individuals with and without asthma during infections with rhinovirus. *Am J Respir Crit Care Med* 2014;189: 532–539.
7. Kim J, Sanders SP, Siekierski ES, Casolaro V, Proud D. Role of NF-κB in cytokine production induced from human airway epithelial cells by rhinovirus infection. *J Immunol* 2000;165:3384–3392.
8. Nakagome K, Bochkov YA, Ashraf S, Brockman-Schneider RA, Evans MD, Pasic TR, *et al*. Effects of rhinovirus species on viral replication and cytokine production. *J Allergy Clin Immunol* 2014;134:332–341.
9. Spurrell JC, Wiehler S, Zaheer RS, Sanders SP, Proud D. Human airway epithelial cells produce IP-10 (CXCL10) *in vitro* and *in vivo* upon rhinovirus infection. *Am J Physiol Lung Cell Mol Physiol* 2005;289: L85–L95.
10. Van Ly D, Faiz A, Jenkins C, Crossett B, Black JL, McParland B, *et al*. Characterising the mechanism of airway smooth muscle β2 adrenoceptor desensitization by rhinovirus infected bronchial epithelial cells. *PLoS One* 2013;8:e56058.
11. Yin FH, Lomax NB. Establishment of a mouse model for human rhinovirus infection. *J Gen Virol* 1986;67:2335–2340.
12. Zambrano JC, Carper HT, Rakes GP, Patrie J, Murphy DD, Platts-Mills TA, *et al*. Experimental rhinovirus challenges in adults with mild asthma: response to infection in relation to IgE. *J Allergy Clin Immunol* 2003;111:1008–1016.
13. Palmenberg AC, Spiro D, Kuzmickas R, Wang S, Djikeng A, Rathe JA, *et al*. Sequencing and analyses of all known human rhinovirus genomes reveal structure and evolution. *Science* 2009;324:55–59.
14. Alper CM, Doyle WJ, Skoner DP, Buchman CA, Seroky JT, Gwaltney JM, *et al*. Prechallenge antibodies: moderators of infection rate, signs, and symptoms in adults experimentally challenged with rhinovirus type 39. *Laryngoscope* 1996;106:1298–1305.
15. Bardin PG, Fraenkel DJ, Sanderson G, van Schalkwyk EM, Holgate ST, Johnston SL. Peak expiratory flow changes during experimental rhinovirus infection. *Eur Respir J* 2000;16:980–985.
16. Cheung D, Dick EC, Timmers MC, de Klerk EP, Spaan WJ, Sterk PJ. Rhinovirus inhalation causes long-lasting excessive airway narrowing in response to methacholine in asthmatic subjects *in vivo*. *Am J Respir Crit Care Med* 1995;152:1490–1496.
17. Christiansen SC, Eddleston J, Bengtson SH, Jenkins GR, Sarnoff RB, Turner RB, *et al*. Experimental rhinovirus infection increases human tissue kallikrein activation in allergic subjects. *Int Arch Allergy Immunol* 2008;147:299–304.
18. Fraenkel DJ, Bardin PG, Sanderson G, Lampe F, Johnston SL, Holgate ST. Lower airways inflammation during rhinovirus colds in normal and in asthmatic subjects. *Am J Respir Crit Care Med* 1995;151: 879–886.
19. Halperin SA, Eggleston PA, Hendley JO, Suratt PM, Gröschel DH, Gwaltney JM Jr. Pathogenesis of lower respiratory tract symptoms in experimental rhinovirus infection. *Am Rev Respir Dis* 1983;128: 806–810.
20. Jarjour NN, Gern JE, Kelly EA, Swenson CA, Dick CR, Busse WW. The effect of an experimental rhinovirus 16 infection on bronchial lavage neutrophils. *J Allergy Clin Immunol* 2000;105:1169–1177.
21. Lemanske RF Jr, Dick EC, Swenson CA, Vrtis RF, Busse WW. Rhinovirus upper respiratory infection increases airway hyperreactivity and late asthmatic reactions. *J Clin Invest* 1989;83: 1–10.
22. Skoner DP, Doyle WJ, Seroky J, Van Deusen MA, Fireman P. Lower airway responses to rhinovirus 39 in healthy allergic and nonallergic subjects. *Eur Respir J* 1996;9:1402–1406.
23. Skoner DP, Whiteside TL, Wilson JW, Doyle WJ, Herberman RB, Fireman P. Effect of rhinovirus 39 infection on cellular immune parameters in allergic and nonallergic subjects. *J Allergy Clin Immunol* 1993;92:732–743.
24. Palmenberg AC, Gern JE. Classification and evolution of human rhinoviruses. *Methods Mol Biol* 2015;1221:1–10.
25. Palmenberg AC, Rathe JA, Liggett SB. Analysis of the complete genome sequences of human rhinovirus. *J Allergy Clin Immunol* 2010;125:1190–1199; quiz 1200–1201.
26. Lethbridge R, Prastanti F, Robertson C, Oo S, Khoo SK, Le Souëf PN, *et al*. Prospective assessment of rhinovirus symptoms and species recurrence in children with and without an acute wheezing exacerbation. *Viral Immunol* 2018;31:299–305.
27. Turunen R, Jartti T, Bochkov YA, Gern JE, Vuorinen T. Rhinovirus species and clinical characteristics in the first wheezing episode in children. *J Med Virol* 2016;88:2059–2068.
28. Ashraf S, Brockman-Schneider R, Bochkov YA, Pasic TR, Gern JE. Biological characteristics and propagation of human rhinovirus-C in differentiated sinus epithelial cells. *Virology* 2013;436:143–149.
29. Ashraf S, Brockman-Schneider R, Gern JE. Propagation of rhinovirus-C strains in human airway epithelial cells differentiated at air-liquid interface. *Methods Mol Biol* 2015;1221:63–70.
30. Griggs TF, Bochkov YA, Nakagome K, Palmenberg AC, Gern JE. Production, purification, and capsid stability of rhinovirus C types. *J Virol Methods* 2015;217:18–23.
31. Xiao Q, Zheng S, Zhou L, Ren L, Xie X, Deng Y, *et al*. Impact of human rhinovirus types and viral load on the severity of illness in hospitalized children with lower respiratory tract infections. *Pediatr Infect Dis J* 2015;34:1187–1192.
32. Koziol-White CJ, Yoo EJ, Cao G, Zhang J, Papanikolaou E, Pushkarsky I, *et al*. Inhibition of PI3K promotes dilation of human small airways in a rho kinase-dependent manner. *Br J Pharmacol* 2016;173: 2726–2738.
33. Cooper PR, Lamb R, Day ND, Branigan PJ, Kajekar R, San Mateo L, *et al*. TLR3 activation stimulates cytokine secretion without altering agonist-induced human small airway contraction or relaxation. *Am J Physiol Lung Cell Mol Physiol* 2009;297:L530–L537.
34. Panettieri RA, Murray RK, DePalo LR, Yadvish PA, Kotlikoff MI. A human airway smooth muscle cell line that retains physiological responsiveness. *Am J Physiol* 1989;256:C329–C335.
35. Balenga NA, Klichinsky M, Xie Z, Chan EC, Zhao M, Jude J, *et al*. A fungal protease allergen provokes airway hyper-responsiveness in asthma. *Nat Commun* 2015;6:6763.

36. Amrani Y, Syed F, Huang C, Li K, Liu V, Jain D, *et al*. Expression and activation of the oxytocin receptor in airway smooth muscle cells: regulation by TNFα and IL-13. *Respir Res* 2010;11:104.
37. Chiba Y, Nakazawa S, Todoroki M, Shinozaki K, Sakai H, Misawa M. Interleukin-13 augments bronchial smooth muscle contractility with an up-regulation of RhoA protein. *Am J Respir Cell Mol Biol* 2009;40: 159–167.
38. Ojiaku CA, Cao G, Zhu W, Yoo EJ, Shumyatcher M, Himes BE, *et al*. TGF-β1 evokes human airway smooth muscle cell shortening and hyperresponsiveness via Smad3. *Am J Respir Cell Mol Biol* 2018;58: 575–584.
39. Tliba O, Deshpande D, Chen H, Van Besien C, Kannan M, Panettieri RA Jr, *et al*. IL-13 enhances agonist-evoked calcium signals and contractile responses in airway smooth muscle. *Br J Pharmacol* 2003;140:1159–1162.
40. Jackson DJ, Makrinioti H, Rana BM, Shamji BW, Trujillo-Torralbo MB, Footitt J, *et al*. IL-33-dependent type 2 inflammation during rhinovirus-induced asthma exacerbations *in vivo*. *Am J Respir Crit Care Med* 2014;190:1373–1382.
41. Shariff S, Shelfoon C, Holden NS, Traves SL, Wiehler S, Kooi C, *et al*. Human rhinovirus infection of epithelial cells modulates airway smooth muscle migration. *Am J Respir Cell Mol Biol* 2017;56:796–803.
42. Lau SK, Yip CC, Lin AW, Lee RA, So LY, Lau YL, *et al*. Clinical and molecular epidemiology of human rhinovirus C in children and adults in Hong Kong reveals a possible distinct human rhinovirus C subgroup. *J Infect Dis* 2009;200:1096–1103.
43. Calhoun WJ, Dick EC, Schwartz LB, Busse WW. A common cold virus, rhinovirus 16, potentiates airway inflammation after segmental antigen bronchoprovocation in allergic subjects. *J Clin Invest* 1994; 94:2200–2208.
44. Miller EK, Hernandez JZ, Wimmenauer V, Shepherd BE, Hijano D, Libster R, *et al*. A mechanistic role for type III IFN-λ1 in asthma exacerbations mediated by human rhinoviruses. *Am J Respir Crit Care Med* 2012;185:508–516.
45. Gerna G, Piralla A, Rovida F, Rognoni V, Marchi A, Locatelli F, *et al*. Correlation of rhinovirus load in the respiratory tract and clinical symptoms in hospitalized immunocompetent and immunocompromised patients. *J Med Virol* 2009;81:1498–1507.
46. Lee GS, Subramanian N, Kim AI, Aksentijevich I, Goldbach-Mansky R, Sacks DB, *et al*. The calcium-sensing receptor regulates the NLRP3 inflammasome through Ca^{2+} and cAMP. *Nature* 2012;492:123–127.
47. Triantafilou K, Kar S, van Kuppeveld FJ, Triantafilou M. Rhinovirus-induced calcium flux triggers NLRP3 and NLRC5 activation in bronchial cells. *Am J Respir Cell Mol Biol* 2013;49:923–934.
48. Zhou Y, Frey TK, Yang JJ. Viral calciomics: interplays between Ca^{2+} and virus. *Cell Calcium* 2009;46:1–17.
49. Adura PT, Reed E, Macintyre J, Del Rosario A, Roberts J, Pestridge R, *et al*. Experimental rhinovirus 16 infection in moderate asthmatics on inhaled corticosteroids. *Eur Respir J* 2014;43:1186–1189.
50. Corne JM, Marshall C, Smith S, Schreiber J, Sanderson G, Holgate ST, *et al*. Frequency, severity, and duration of rhinovirus infections in asthmatic and non-asthmatic individuals: a longitudinal cohort study. *Lancet* 2002;359:831–834.
51. Chambers LS, Black JL, Ge Q, Carlin SM, Au WW, Poniris M, *et al*. PAR-2 activation, PGE2, and COX-2 in human asthmatic and nonasthmatic airway smooth muscle cells. *Am J Physiol Lung Cell Mol Physiol* 2003;285:L619–L627.
52. Chin LY, Bossé Y, Pascoe C, Hackett TL, Seow CY, Paré PD. Mechanical properties of asthmatic airway smooth muscle. *Eur Respir J* 2012;40:45–54.
53. Léguillette R, Lauzon AM. Molecular mechanics of smooth muscle contractile proteins in airway hyperresponsiveness and asthma. *Proc Am Thorac Soc* 2008;5:40–46.
54. Ma X, Cheng Z, Kong H, Wang Y, Unruh H, Stephens NL, *et al*. Changes in biophysical and biochemical properties of single bronchial smooth muscle cells from asthmatic subjects. *Am J Physiol Lung Cell Mol Physiol* 2002;283: L1181–L1189.
55. Roth M, Johnson PR, Borger P, Bihl MP, Rüdiger JJ, King GG, *et al*. Dysfunctional interaction of C/EBPα and the glucocorticoid receptor in asthmatic bronchial smooth-muscle cells. *N Engl J Med* 2004;351: 560–574.
56. Trian T, Burgess JK, Niimi K, Moir LM, Ge Q, Berger P, *et al*. β_2-Agonist induced cAMP is decreased in asthmatic airway smooth muscle due to increased PDE4D. *PLoS One* 2011;6:e20000.